A multi-scale and multi-instrument approach to understanding the deportment of Co, Bi and Ag in the Swartberg polymetallic sulphide ore

S Burness[a*], A Mulelu[a], T Molaolwe-Dipitso[b], W Price[c], A Menzies[d], M. Becker[a]

[a]*Centre for Minerals Research, University of Cape Town, Rondebosch, Cape Town 7700, South Africa*
[b]*Black Mountain Mine, Vedanta Group International, Aggeneys 8893, South Africa.*
[c]*Deputy Head of Exploration, Vedanta Zinc International (Vedanta Resources Limited), South Africa*
[d]*Bruker Nano Analytics GmbH, AmStudioD, 12489 Berlin, Germany*

**Corresponding author: sara.burness@uct.ac.za*

1. Introduction

The Aggeneys-Gamsberg Ore District (A-GOD) in north-western South Africa comprises several world-class Broken Hill-type deposits, including the Pb-Zn-Cu-Ag-rich Swartberg and Deeps deposits and the Zn-Pb-Ba-rich Gamsberg deposit. This paper focuses on the Swartberg ore, which has historically been processed as a blend with Deeps ore at the Black Mountain Mines (BMM) Concentrator through sequential flotation stages. With the closure of the Deeps mine due to ore depletion, the key interest is to understand the variability of the Swartberg deposit, as this represents a key future resource to the company (Estimated 175.4 Mt resource and reserve, at 0.3% Cu, 1.8% Pb, 0.7% Zn, 34g/t Ag; VZI, 2026).

Prior process mineralogical studies have largely focused on the valuable sulphide mineralogy and liberation, with limited focus on trace element variability (Rudnick & Rozendaal, 2013). This is largely due to the time and cost required to generate robust datasets to understand trace element variability, where the key trace elements are either byproducts or penalty elements. Here, we focus on the trace element variability of three trace elements: silver, cobalt and bismuth. All three elements appear as critical raw materials on the European Union list (European Commission, 2026), although only Co appears on the South African critical raw material list (Department of Mineral and Petroleum Resources [DMPR], 2025). In the case of Ag, a typical Pb concentrate must exceed 50 g/t Ag, and similarly, a Zn concentrate must exceed 93 g/t Ag for payable credits (Teck Resources Limited, 2015). For Co, however, the preferred maximum limit for a Zn concentrate is 200 g/t and above this amount, penalties apply because it interferes with the purity of the final saleable zinc cathode (Sinclair, 2005). Bi in Pb concentrates can be penalised anywhere between 100-300 g/t depending on the details of the smelter contract (Noakes & Lanz, 1993). To optimise processing of these ores, a comprehensive understanding of trace element variability is required, so appropriate strategies can be implemented to maximise the value of the resource.

The Swartberg deposit comprises two main mineralised horizons: an Upper Ore Body (UOB), which is up to ~20 m thick, dominated by sulphide- and magnetite-rich iron formations with associated hematite-

barite and mixed siliciclastic units; and a thinner Lower Ore Body (LOB), typically 3–6 m thick, consisting of fine-grained pelitic pyritic schist with minor magnetite and barite. The ore bodies are separated by quartz-rich metasedimentary units that include a garnet-bearing quartzite lens, interpreted as a metamorphosed pelitic marker horizon and locally associated with Cu-rich (chalcopyrite-bearing) mineralisation (Rozendaal et al., 2017; Gordon et al., 2021).

Previous studies have shown that Ag in Swartberg ores (Table 1) occurs both in discrete Ag-bearing minerals (e.g. acanthite, pyrargyrite and freibergite) associated with base-metal sulphides, and in solid solution within galena, chalcopyrite and Fe-sulphides (e.g., Burness et al., 2024; Rudnick & Rozendaal, 2013; Rudnick, 2016; Williams & Holtzhausen, 2001). These different modes of occurrence have implications for Ag deportment and its potential for selective recovery. By contrast, cobalt displays a more complex deportment: fine-grained discrete Co-minerals (<10 µm) are mainly reported from the upper ore body while Co also occurs in solid solution within pyrrhotite and sphalerite. In the LOB, Co is largely incorporated in Mn-rich sphalerite and pyrite, limiting selective rejection and increasing the risk of Co reporting to concentrate as a low-grade penalty element (Cawood & Rozendaal, 2020). Williams and Holtzhausen (2001) reported discrete cosalite and lesser bismuthinite associated with both chalcopyrite and galena as the main Bi hosts in their study of various Swartberg flotation concentrates.

Table 1: List of discrete Co, Ag and Bi minerals previously identified in Swartberg ore (From: Burness et al 2024, Rudnick & Rozendaal, 2013, Rudnick, 2016, Williams & Holtzhausen, 2001).

Trace element	**Mineral**	**Composition**
Co	Smaltite	$(Co,Fe,Ni)As_2$
	Glaucodot	$(Co,Fe)AsS$
	Cobaltite	$CoAsS$
	Co-pyrite	$(Fe,Co)S_2$
	Costibite	$CoSbS$
	Co-pentlandite	$(Fe,Ni,Co)_9S_8$
	Alloclasite	$CoAsS$
	Safflorite	$(Co,Fe)As_2$
Ag	Malinowskite	$Ag_{21.5}Cu_{3.53}Pb_{5.1}S_{18}$
	Freibergite - pyrargyrite	$(Ag,Cu,Fe)_{12}(Sb,As)_4S_{13}$ -Ag_3SbS_3
	Stromeyerite - sternbergite	$AgCuS$
	Acanthite	Ag_2S
	Sternbergite	$AgFe_2S_3$
	Apthonite	$(Cu, Zn, Ag, Fe)_{12}Sb_4S_{13}$
	Jalpaite	Ag_3CuS_2
	Pearceite-polybasite	$[Ag_9CuS_4][(Ag,Cu)_6[As, Sb)_2S_7]$
Bi	Cosalite	$Pb_2Bi_2S_5$
	Bismuthinite	Bi_5S_3

However, the quantitative mineralogical deportment of Ag and Co in the Swartberg LOB remains poorly constrained. This study uses a multi-scale, multi-instrument approach to investigate the deportment of Ag, Co and Bi in the Swartberg lower ore body (LOB) using both drill core and milled flotation feed. Using complementary X-ray and electron beam techniques (micro-XRF, Auto-SEM-EDS and EPMA), together with laser-based analysis (LA-ICP-MS), this study identifies the mineralogical hosts and textural associations of these trace elements to understand how these characteristics may influence liberation, recovery and potential selective extraction.

2. Materials and Methods

Figure 1 summarises the overall workflow used to characterise trace element distribution in this study, highlighting how the various methods complement one another by covering both bulk and in-situ analysis at both the meso- and micro-scales.

2.1 Sampling and sample preparation

Ten drill core samples were collected from the Eastern, Western and Northern parts of the Swartberg lower ore body. The cores intersected a range of lithologies, including interbanded muscovite-quartz schist, chlorite schist and sulphidic quartzite. Two areas of interest per core were prepared as 30 mm polished resin blocks for automated mineralogical (QEMSCAN), electron probe microanalysis (EPMA) and laser ablation inductively coupled plasma-mass spectrometry (LA-ICP-MS) analysis, with the remaining material retained for micro-XRF analysis. Additional drill core material was composited to generate three ‘bulk’ samples that were milled to a p80 ~75 µm. This material was subsampled for quantitative X-ray diffraction (XRD) and QEMSCAN trace mineral searches. The remaining material was thereafter wet-screened into five size fractions. Material from each of the size fractions was submitted for chemical assays and further QEMSCAN analysis. All the milled QEMSCAN samples were prepared as vertical/transverse sections for QEMSCAN analysis.

2.2 Chemical assays

The milled, sized samples were analysed at BMM using inductively coupled plasma optical emission spectrometry (ICP-OES) for Cu, Pb, Zn, Fe and Mn, and atomic absorption spectrometry (AAS) for Ag, Co and Bi. Major element assays were essential for validating the QEMSCAN-measured mineral grades.

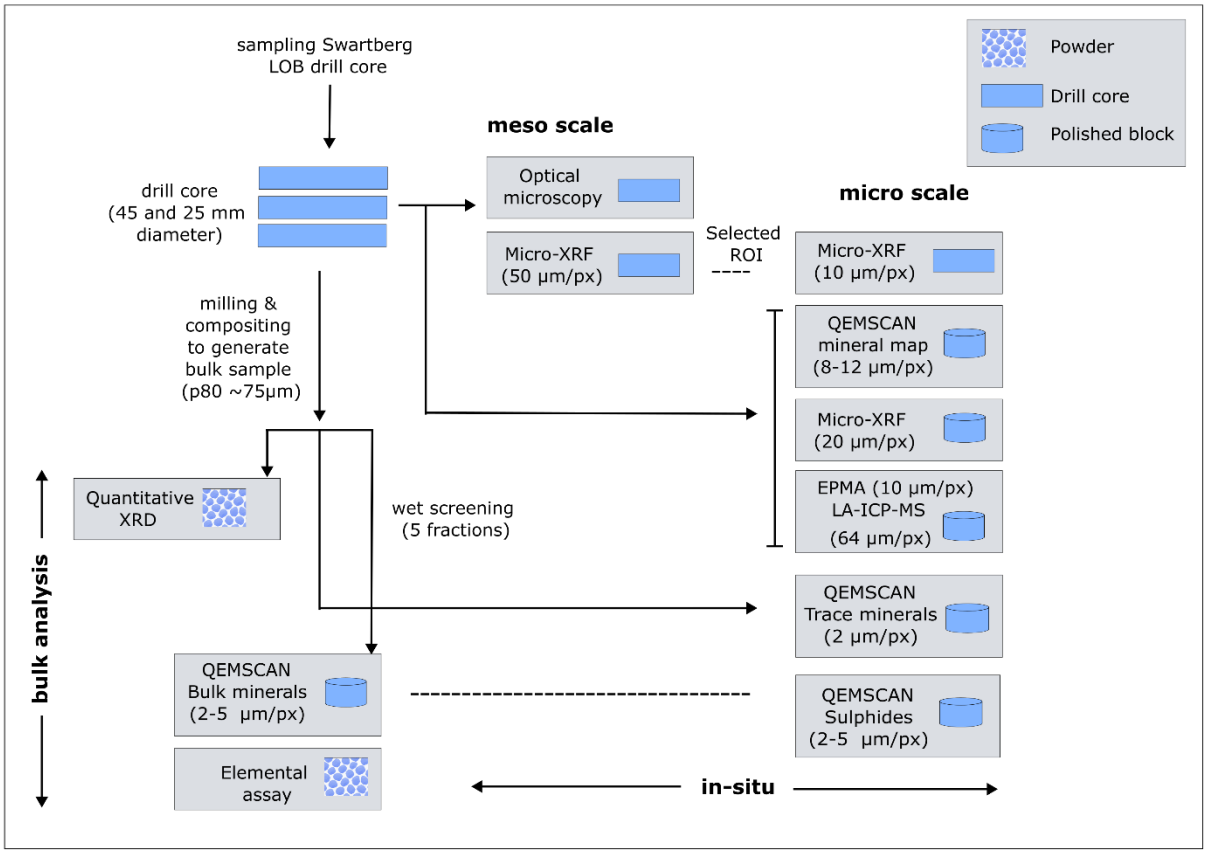

Figure 1: Workflow used to characterise and quantify the deportment of Ag, Co and Bi in this study.

2.3 Mineralogical measurements

The drill core samples were run on an FEI QEMSCAN 650F at UCT operating at 25 kV and 10 nA using the field image measurement routine (1500-2000 µm field size and 8-12 µm pixel spacing). Milled and sized samples were analysed using the bulk mineralogical analysis (BMA) routine, whereas unsized samples were analysed using the trace mineral search (TMS) routine (2 µm point spacing) to identify discrete Ag-, Co- and Bi-bearing minerals. Selected discrete phases were analysed by SEM energy-dispersive spectrometry (SEM-EDS) to confirm mineral identity.

Micro-XRF analysis was performed using a Bruker M4 Tornado Plus micro-XRF instrument housed at Bruker Nano Analytics (Berlin, Germany) to perform in situ elemental analyses on selected drill-core samples across representative lithological units. The quarter-cores under investigation were mapped in a single scan using beam conditions of 50 kV and 600 µA, a pixel acquisition time of 10 ms, and at various pixel sizes of 50, 20, and 10 µm. Results include the spatial elemental variations of major and trace elements, including Pb, Zn, S, Co, Ag and Bi. These were processed using standard background correction and peak deconvolution routines. False-colour elemental maps were generated to visualise geochemical distributions, and total X-ray intensity maps were used to support phase identification and textural interpretation. High-resolution mapping at 10 µm was conducted on selected Ag grains. Micro-

XRF was also conducted on the QEMSCAN 30 mm field image blocks for false-colour maps comparable to those generated by QEMSCAN, and to determine the distribution of Ag, Co and Bi across the images. The blocks were mapped at the same beam conditions as the drill cores, but at 20 µm pixel spacing.

Laser Ablation Inductively Coupled Plasma Mass Spectrometry (LA-ICP-MS) analyses were performed at UCT using a RESOlution 193-nm excimer laser coupled to an iCAP RQ ICP-MS. Analyses were conducted using a 64 µm spot size at 10 Hz and a fluence of 4.7 J cm^{-2}, with sulphur (^{32}S) as the internal standard. Instrument calibration and data quality were monitored using the Mass-1 synthetic Fe–Zn–Cu sulphide reference material (USGS; Wilson et al., 2002), and data reduction was performed using LadR software with correction for argide interferences. Five to seven spots were analysed per mineral per sample.

Representative samples were selected for electron probe microanalysis (EPMA). Analyses were conducted using a JEOL JXA-iSP100 Super Probe at UCT. Prior to analysis, polished sections were carbon-coated. Quantitative analyses were performed using wavelength-dispersive spectrometry (WDS) with a 15 kV accelerating voltage, 20 nA beam current, 11 mm working distance and ~ 1 µm spot size. Appropriate mineral and pure metal standards were used for calibration. In addition to trace-element quantification, backscattered electron (BSE) imaging was used to investigate sulphide textures, exsolution features, and multiple sulphide generations, providing critical textural context to support mineralogical interpretations. Five to seven spots were analysed per mineral per sample.

3. Results and Discussion

3.1 Element and mineral grades of milled samples

Overall, the three samples share similar mineralogy and are dominated by quartz, mica and pyrite (Figure 2), with lesser kaolinite, chlorite, garnet and magnetite. In terms of valuable sulphides, West contains the highest galena content (6.4 wt.%), followed by East (4.8 wt.%) and North (2.1 wt.%). East has the highest sphalerite grade (12.7 wt.%), with West and North having similar grades around 5 wt.%. Chalcopyrite contents in all three samples are low (< 0.5 wt.%). Although present in all samples, secondary sulphates (jarosite and aluminite) had the highest grades in the West (6.1 wt.%) compared with < 1 wt.% in the East and North. Cu, Pb and Zn grades summarised in Table 2 support these observations. In terms of trace elements, Co grades were highest in the East (108.5 g/t), with West and North having similar Co grades around 33 g/t. Ag grades were highest in the West and East (62.2-73.2 g/t), with North Ag grades being significantly lower (25.5 g/t). Bi grades follow the opposite trend, with West and East showing the lowest grades (~ 7 g/t) compared with North (28.5 g/t).

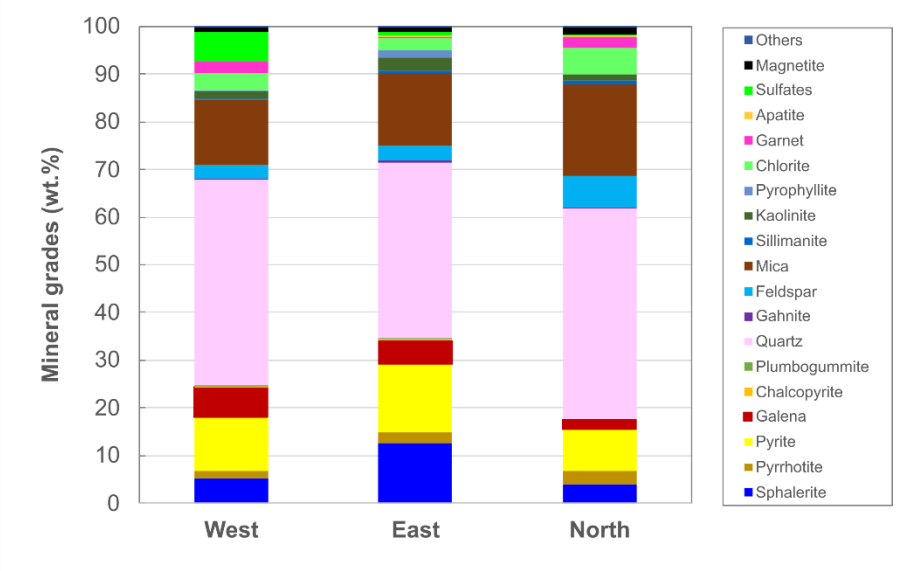

Figure 2: Bulk mineralogy of the Swartberg milled samples.

Table 2: Bulk elemental grades of the Swartberg milled samples. All elements are given in wt.% unless otherwise indicated.

Sample	Cu	Pb	Zn	Fe	Mn	Ag (g/t)	Co (g/t)	Bi (g/t)	Cd (g/t)
West	0.1	4.2	3.1	9.8	0.2	62.2	32.6	7.6	293.7
East	0.2	3.4	7.1	10.3	0.1	73.2	108.5	6.1	347.9
North	0.1	1.4	2.3	8.9	0.1	25.5	33.4	28.5	88.0

Examination of the size-by-size distributions of the base-metal sulphides relative to key elements reveals clear differences in the deportment behaviour of Ag, Co and Bi. Silver (Ag) shows a strong association (Figure 3a) with Pb (galena) and Cu (chalcopyrite), respectively. More than 35% of the Ag, together with about 50% of the galena and 40-46% of the chalcopyrite, report to the −10 µm fraction, indicating fine-grained mineralisation, and if any discrete Ag minerals are present, associated with either galena or chalcopyrite, they are likely very fine. For North, more than 46% of the galena occurs in the -10 µm fraction. Ag shows a weaker association with sphalerite and Zn. Bi exhibits a distribution similar to that of galena, as indicated by the overlapping Pb and Bi trends. The Bi and Cu distribution trends also show similarities, with the distribution of bismuth corresponding to that of chalcopyrite. This may indicate that bismuth occurs in solid solution within chalcopyrite, although the EPMA and laser ablation analyses would be required to confirm this.

In contrast, the size-by-size distribution of Co (Figure 3b) shows a strong association with pyrite, chalcopyrite (Cu) and sphalerite (Zn), particularly in the East and West samples. Approximately 40% of the sphalerite reports to the −10 µm fraction, with a further ~25% in the +38 µm fraction in the West

and East samples (i.e., a bi-modal distribution). For pyrite, up to ~20% occurs in the −10 µm fraction, while ~35% reports to the +38 µm fraction. For Cu, on average 42% reports to the -10 µm fraction, with 25% occurring in +38 µm for West and East. These size fractions coincide with high Co grades, which suggests that Co may be predominantly hosted in solid solution within these sulphides, rather than occurring as discrete Co-minerals.

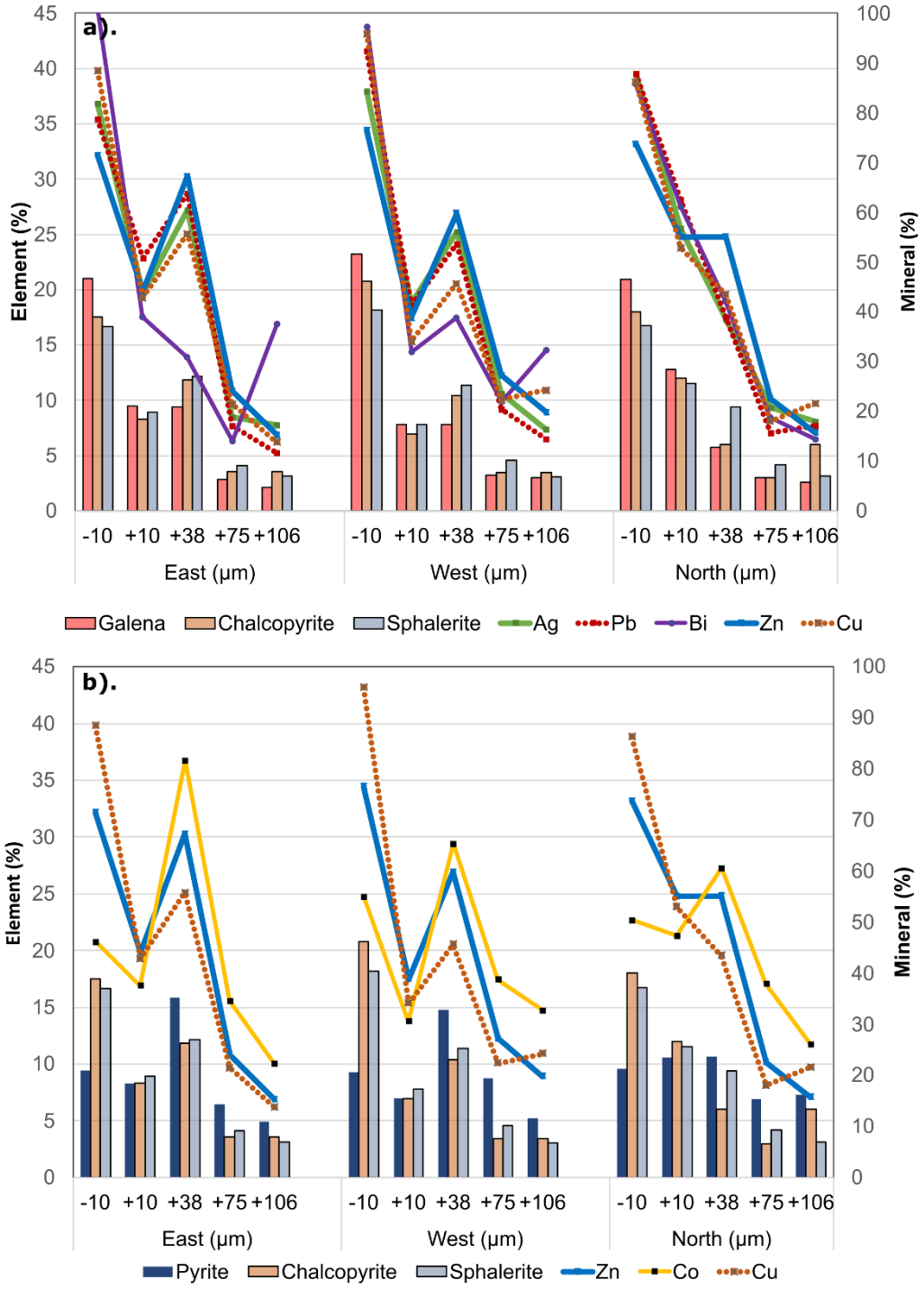

Figure 3: Size-by-size normalised distribution of key elements (left vertical axis) and sulphides (right vertical axis) in the milled samples focusing on Ag, Bi (a) and Co (b) associations.

4. Preliminary findings and next steps

Preliminary findings indicate similarities in trends between the East and West samples regarding element deportment, whereas North material has more complex deportment patterns. Understanding the size-by-size distribution of key elemental and mineral grades provides some insights into trace element deportment, but no information on whether these elements occur in discrete trace mineral phases or are hosted in solid solution substitution in common sulphide minerals. This outlines the limitations of bulk analysis methods and demonstrates the need for complementary meso- and micro-scale in-situ measurements to provide this information.

5. Acknowledgements

Grateful thanks are given to Vedanta Zinc International for their financial and logistical support of this work, and to Bruker Nano Analytics GmbH, Germany, for access to their M4 Tornado Plus micro-XRF instrument. Various staff members at UCT are acknowledged for their assistance with sample preparation and data acquisition.

6. References

Burness, S., Mulelu, A. & Becker, M. (2024). Distribution of cobalt in Black Mountain Mines samples. Unpublished internal report prepared for Vedanta Zinc International, Centre for Minerals Research, University of Cape Town, Cape Town, South Africa.

Cawood, K.T. & Rozendaal, A. (2020). A multistage genetic model for the metamorphosed Mesoproterozoic Swartberg base metal deposit, Aggeneys-Gamsberg Ore District, South Africa. Economic Geology, 115(5), 1021-1054.

Department of Mineral and Petroleum Resources. (2025). Critical minerals and metals strategy for South Africa. Pretoria: Department of Mineral and Petroleum Resources.

European Commission. (2026). Raw Materials Information System (RMIS): Raw materials' profiles. Joint Research Centre. Available at: https://rmis.jrc.ec.europa.eu/rmp/ (Accessed: 13 October 2026).

Gordon, H.J.J., Stroebel, G., Miller, J.A., Corin, K.C., Landsberg, A.E. & Becker, M. (2021). Process mineralogical characterization of the Swartberg polymetallic sulfide ore, South Africa. In: Proceedings of the XXX International Mineral Processing Congress (IMPC 2020). Cape Town, South Africa: Southern African Institute of Mining and Metallurgy (SAIMM).

Noakes, M. & Lanz, T. (1993). Cost estimation handbook for the Australian mining industry. Australia: Australasian Institute of Mining and Metallurgy.

Rudnick, T.K. & Rozendaal, A. (2013). Genesis of the stratiform BH-t Swartberg Cu-Pb-Zn-Ag deposit, Northern Cape, South Africa. In: 12th Biennial SGA Meeting Conference Proceedings. Uppsala, Sweden.

Rudnick, T.K. (2016). The Genesis of the Swartberg Base-Metal Sulphide Deposit, South Africa. Unpublished master's thesis, Stellenbosch University, Stellenbosch, South Africa. Available at: http://hdl.handle.net/10019.1/100381 (Accessed: 27 October 2026).

Rozendaal, A., Rudnick, T.K. & Heyn, R. (2017). Mesoproterozoic base metal sulphide deposits in the Namaqua sector of the Namaqua-Natal Metamorphic Province, South Africa: A review. South African Journal of Geology, 120(1), 153-186.

Sinclair, R.J. (2005). The extractive metallurgy of zinc. Victoria: Australasian Institute of Mining and Metallurgy.

Teck Resources Limited. (2015). Modelling Workshop. Investor presentation, 4 November 2015. Available at: https://www.teck.com/media/Investors-Presentations-Webcasts-20151104-modelling-workshop.pdf (Accessed: 13 April 2026).

Vedanta Zinc International. (2026). Black Mountain Mines Internal Report.

Williams, N.R. & Holtzhausen, L.S. (2001). The impact of ore characterization and blending on metallurgical plant performance. Journal of the South African Institute of Mining and Metallurgy, 101(8), 437-443.

Wilson, S.A., Ridley, W.I. & Koenig, A.E. (2002). Development of sulfide calibration standards for the laser ablation inductively coupled plasma mass spectrometry technique. Journal of Analytical Atomic Spectrometry, 17(4), 406-409.